NeuroImage **10,** 63–83 (1999)
Article ID nimg.1999.0440, available online at http://www.idealibrary.com on IDEAL®

Areas 3a, 3b, and 1 of Human Primary Somatosensory Cortex

1. Microstructural Organization and Interindividual Variability

Stefan Geyer,* Axel Schleicher,† and Karl Zilles*,†,‡

Department of Neuroanatomy and †C. and O. Vogt Brain Research Institute, University of Düsseldorf, P.O. Box 10 10 07, 40001 Düsseldorf, Germany; and ‡Institute of Medicine, Research Center Jülich, 52425 Jülich, Germany

Received June 2, 1998

This study defines cytoarchitectonic areas 3a, 3b, and 1 of the human primary somatosensory cortex by objective delineation of cytoarchitectonic borders and ensuing cytoarchitectonic classification. This avoids subjective evaluation of microstructural differences which has so far been the only way to structurally define cortical areas. Ten brains were fixed in formalin or Bodian's fixative, embedded in paraffin, sectioned as a whole in the coronal plane at 20 µm, and cell stained. Cell bodies were segmented from the background by adaptive thresholding. Equidistant density profiles (125 µm wide, spacing 300 or 150 µm) were extracted perpendicularly to the pial surface across cortical layers II–VI and processed with multivariate statistical procedures. Positions of significant differences in shape between adjacent groups of profiles were correlated with the cytoarchitectonic pattern. Statistically significant borders can be reproduced at corresponding positions across a series of nearby sections. They match visible changes in cytoarchitecture in the cell-stained sections. Area 3a lies in the fundus of the central sulcus, and area 3b in the rostral bank of the postcentral gyrus. Area 1 lies on its crown and reaches down into the postcentral sulcus. Interareal borders, however, do not match macrostructural landmarks of the postcentral gyrus, and they considerably vary in their positions relative to these landmarks across different brains. Hence, only genuine microstructural analysis can define the borders between these cortical areas. Additional significant borders which do not correlate with visible changes in cytoarchitecture can be found within areas 3b and 1. They may represent somatotopy and/or cortical representations of different somatosensory receptors. © 1999 Academic Press

INTRODUCTION

Several microstructural maps of the human primary somatosensory cortex (S1) have been published (Brodmann, 1909; Vogt and Vogt, 1919; von Economo and Koskinas, 1925; Bailey and von Bonin, 1951; Sarkissov *et al.*, 1955; Braak, 1980; White *et al.*, 1997). Most authors agree as to the number, microstructural features, and extent of areas within S1 (i.e., areas 3a, 3b, 1, and 2 according to the nomenclature of Brodmann (1909) and Vogt and Vogt (1919) which is most widely used). Area 3a lies in the fundus of the central sulcus, area 3b occupies mainly the rostral bank, area 1 occupies the crown, and area 2 occupies the caudal bank of the postcentral gyrus. Unfortunately, microstructural maps of different authors vary in many details. This is due to interindividual variability and the small number of brains examined in each study (i.e., the problem of sample size) which should be seen, however, in the light of the enormous size of the human brain and the time-consuming and cumbersome procedure of microstructural parcellation. Another problem is the inherent subjectivity underlying any microstructural parcellation of the cerebral cortex. Up to now, it has not been possible to define microstructural borders between cortical areas in an objective and observer-independent way. Instead, numerous subjective factors, e.g., experience and technique of pattern recognition, have influenced the results and introduced a significant degree of intra- and interobserver variability. This led to a long-standing polemic between two extreme tenets in the first decades of this century: those investigators who advocated "haarscharfe Grenzen" (i.e., boundaries as sharp or fine as a hair) between cortical areas (to paraphrase O. Vogt) and those researchers who interpreted the cortex as a more or less homogeneous matrix with only minor variations (to paraphrase P. Bailey and G. von Bonin). Severe criticism of cytoarchitectonic parcellation studies (Lashley and Clark, 1946) was the consequence.

On the other hand, there is evidence from many recent electrophysiological studies in S1 of nonhuman primates that neurons with similar receptive fields and response properties lie within the same cytoarchitectonic area when the identical brain is sectioned and cell-stained following recording experiments, and penetration sites are correlated with the cytoarchitectonic

1053-8119/99 $30.00

pattern. Conversely, response properties of neurons change across cytoarchitectonic borders (Merzenich *et al.*, 1978; Kaas *et al.*, 1979; Iwamura *et al.*, 1980, 1983a,b, 1985, 1993, 1994). Cortical areas which are different from each other in their cytoarchitectonic patterns also differ from each other in their electrophysiological properties or, in other words, microstructure indeed parallels function.

In humans, noninvasive imaging techniques, e.g., positron emission tomography (PET), functional magnetic resonance imaging (fMRI), or magnetoencephalography (MEG), functionally parcellate S1 with increasing spatial resolution, but they relate foci of cerebral activation only to macrostructural landmarks of the cortex, i.e., gyri and sulci. On the other hand, structural–functional correlations in primate S1 (see above) and other cortical regions as well show that cortical areas as functional entities can be defined as to their location and extent only microstructurally, e.g., by cytoarchitecture. Unfortunately, most microstructurally defined interareal borders do not match macrostructural landmarks of the human cortex and are quite variable as to their location and extent across individuals (Rademacher *et al.*, 1993; Roland and Zilles, 1994, 1996; Geyer *et al.*, 1995, 1996, 1997; Rajkowska and Goldman-Rakic, 1995; Simon *et al.*, 1995; Morosan *et al.*, 1996; Rademacher *et al.*, 1996; White *et al.*, 1997; Roland *et al.*, 1997; Zilles *et al.*, 1997; Amunts *et al.*, 1997). For this reason, structural–functional correlations based only on macrostructure are questionable and may account for at least some of the conflicting results functional imaging studies have provided in recent years, e.g., the debate whether (Hallett *et al.*, 1994; Stephan *et al.*, 1995; Sabbah *et al.*, 1995; Leonardo *et al.*, 1995; Roth *et al.*, 1996; Porro *et al.*, 1996) or not (Roland *et al.*, 1980; Rao *et al.*, 1993; Decety *et al.*, 1994; Sanes, 1994; Parsons *et al.*, 1995) primary sensorimotor cortex is activated during imagined movements.

Thus, two things are needed: (i) objective cytoarchitectonic mapping and delineation of cortical areas in order to avoid subjective evaluation of microstructural differences between areas (including all problems related to it) and (ii) transfer of these areas into a standardized 3-D reference system on the basis of a computerized brain atlas (Roland and Zilles, 1994) in which they can be matched with functional data, e.g., from PET, fMRI, or MEG.

In this study we used a new approach (Schleicher *et al.*, 1995, 1999), i.e., a combination of objective delineation of cytoarchitectonic borders followed by cytoarchitectonic classification to delineate areas 3a, 3b, and 1 of human S1 in 10 postmortem brains. As a next step, these areas will be transformed into the standard anatomical format of the computerized *Human Brain Atlas* (Roland and Zilles, 1994), and corresponding areas from different brains will be superimposed in 3-D space. This is the basis for subsequent probabilistic *microstructural*–functional correlation with data obtained from, e.g., PET (Geyer *et al.*, 1997).

TABLE 1

Brains Used for Cytoarchitectonic Mapping of Areas 3a, 3b, and 1

Brain	Sex	Age (years)	Cause of death	Post mortem delay (h)	Fixative
207/84	Male	75	Toxic glomerulonephritis	24	Formalin
544/91	Female	79	Carcinoma of the bladder	24	Bodian
281/93	Male	68	Vascular disease	16	Formalin
189/92	Male	55	Carcinoma of the rectum	24	Formalin
68/95	Female	79	Cardiorespiratory insufficiency	16	Bodian
14/94	Female	43	Pulmonary embolism	24	Formalin
2/95	Female	85	Mesenteric artery infarction	14	Bodian
382/81	Female	59	Cardiorespiratory insufficiency	24	Formalin
56/94	Female	72	Renal failure	12	Formalin
2431	Male	39	Drowning	10	Formalin

MATERIALS AND METHODS

Histological Processing of the Brains

Cytoarchitectonic analysis was done in 10 postmortem brains obtained at autopsy from subjects with no known history of neurological or psychiatric diseases (4 male and 6 female, mean age 65.4 years, range 39–85 years; cf. Table 1). All subjects had given written consent before death and/or had been included in the body donor program of the Brain Research Institute, University of Düsseldorf, Germany. The brains were removed from the skull and were fixed in 4% formaldehyde diluted in water or in Bodian's fixative (90 ml of 80% ethanol, 5 ml of 37% formaldehyde diluted in water, and 5 ml of glacial acetic acid) for 5 months. The brains were fixed in a freely floating way, i.e., suspended at the basilar artery, to avoid compression or distortion during fixation. The arachnoidea was removed after fixation. The brains were then dehydrated in graded alcohols, embedded in a paraffin block, and sectioned at 20 μm in a coronal plane with a microtome for large sections. Sections were mounted on gelatin-coated slides and were stained with a modified silver method (Merker, 1983) which yields Nissl-like, high-contrast staining for cytoarchitectonic analysis.

Objective Delineation of Cytoarchitectonic Borders and Cytoarchitectonic Classification

Rectangular regions of interest (ROI) covering the caudal bank of the precentral gyrus and the rostral and caudal banks of the postcentral gyrus were defined in each selected cell-stained section. These ROIs were scanned in a mosaic-like sequence with a digital camera (XC-75; Sony, Tokyo, Japan; image matrix 512 × 512 pixels, 8-bit gray value resolution) attached to a microscope (Universal microscope; Zeiss, Oberkochen, Germany) which was equipped with a computer-controlled motorized stage. The images (square microscopical field 550 µm across) were transferred to a computer and further processed with an image analysis software package (KS 400; Zeiss). In each image, the areal fraction of darkly stained cell bodies was measured after adaptive thresholding (Schleicher and Zilles, 1990) in square, adjoining fields 25 µm wide. This areal fraction [gray level index (GLI)] is highly correlated with the volume density of neurons (Wree *et al.*, 1982). Glial and endothelial cells are equally distributed throughout the layers of the cortex and are therefore an additive, yet constant, contribution to the volume density of neurons. The GLI was measured in each field within each image; the resulting data matrix covering the entire ROI is the GLI image. Variations in staining intensities of cell bodies and/or background do not influence the GLI image because the GLI is extracted from binary images. For further details see Schleicher and Zilles (1990).

Equidistant density profiles [125 µm wide; spacing between adjacent profiles 300 µm (for low spatial resolution) or 150 µm (for high resolution)] covering the entire ROI were extracted from the GLI images perpendicularly to a central line between layers I/II and layer VI/white matter. Profiles extended from the border between layers I and II to the border between layer VI and white matter. An outer (between layers I and II) and inner (between layer VI and white matter) contour line was defined interactively in each GLI image with a graphics tablet. The central line between both contour lines was calculated with a skeleton algorithm, and equidistant profiles (spacing along the central line 300 or 150 µm) were automatically extracted from the GLI image. Each profile was oriented perpendicularly to the central line, and extended from the outer to the inner contour line.

Profiles were standardized to a length of 101 GLI values (corresponding to a cortical depth of 100%) by resampling the data with linear interpolation in order to compensate for variations in cortical thickness. Profile shapes were quantified by extracting 10 features (mean y, mean x, standard deviation of x, skewness, kurtosis) from each standardized profile and from the absolute value of its first derivative and were combined into one feature vector $\mathbf{X}$. The data from the sample of n profiles per ROI were standardized to z-scores in order to assign equal weight to each of the features. A mean feature vector $\overline{\mathbf{X}_1}$ was calculated from a block of b_1 adjacent profiles ($8 \leq b_1 \leq 20$) and another mean feature vector $\overline{\mathbf{X}_2}$ from a neighboring block of b_2 adjacent profiles ($8 \leq b_2 \leq 20$; $b_1 = b_2$). The Mahalanobis distance (Mahalanobis *et al.*, 1949) $D^2 = (\overline{\mathbf{X}_1} - \overline{\mathbf{X}_2})' \mathbf{C}^{-1} (\overline{\mathbf{X}_1} - \overline{\mathbf{X}_2})$ was calculated from the mean vectors and the inverse of the pooled covariance matrix $\mathbf{C}^{-1}$. D^2 values were plotted as a function of the positions of the profile blocks relative to the cortex (see Fig. 3). The resulting distance function revealed maxima at locations at which regions covered by profiles showed marked differences in laminar patterns. Statistical significance was established by calculating Hotelling's statistic $T^2 = (D^2/(1/b_1 + 1/b_2))$ ($b_1 = b_2$, the number of profiles per block). The corresponding p values were Bonferroni corrected for multiple comparisons. The number of profiles per block b defined the spatial resolution of this procedure, i.e., only cytoarchitectonic entities wider than the cortical sector covered by one block of profiles could be resolved with correct distance values. For this reason, significant maxima of the distance function D^2 were defined in the following way: (1) Maxima with $p \geq 0.05$ were discarded. (2) If the distance between two adjacent maxima was equal to or smaller than one block of profiles, the maximum with the higher p value was discarded. The procedure converged after a second pass of step (2). The remaining maxima were termed "main maxima." For each ROI, distance functions were calculated for $b = 8$ to $b = 20$, and positions of main maxima were plotted as a function of b (see Figs. 4, 8, and 10). For further details see Schleicher *et al.* (1999). The positions of these main maxima were compared with the visible cytoarchitectonic pattern in the cell-stained sections.

A discriminant analysis was performed for each sample of n profiles per ROI to analyze differences in shapes between those groups of profiles which had been extracted from areas 4, 3a, 3b, 1, and 2. The result of each analysis was plotted using the first two canonical variables (see Fig. 12). These variables are the x- and y-axes of a plane which shows most clearly differences between groups of profiles sampled from the five areas.

RESULTS

Two examples of cell-stained coronal whole brain sections from two different brains (comparable levels in the rostrocaudal direction) are shown in Fig. 1 [brain 207/84, section 3301 (Fig. 1A), and brain 544/91, section 3241 (Fig. 1B)]. Boxes show ROIs covering the caudal bank of the precentral gyrus (pr) and the rostral and caudal banks of the postcentral gyrus (po) which were used for GLI measurements and subsequent extraction of profiles. The ROI from brain 207/84, section 3301

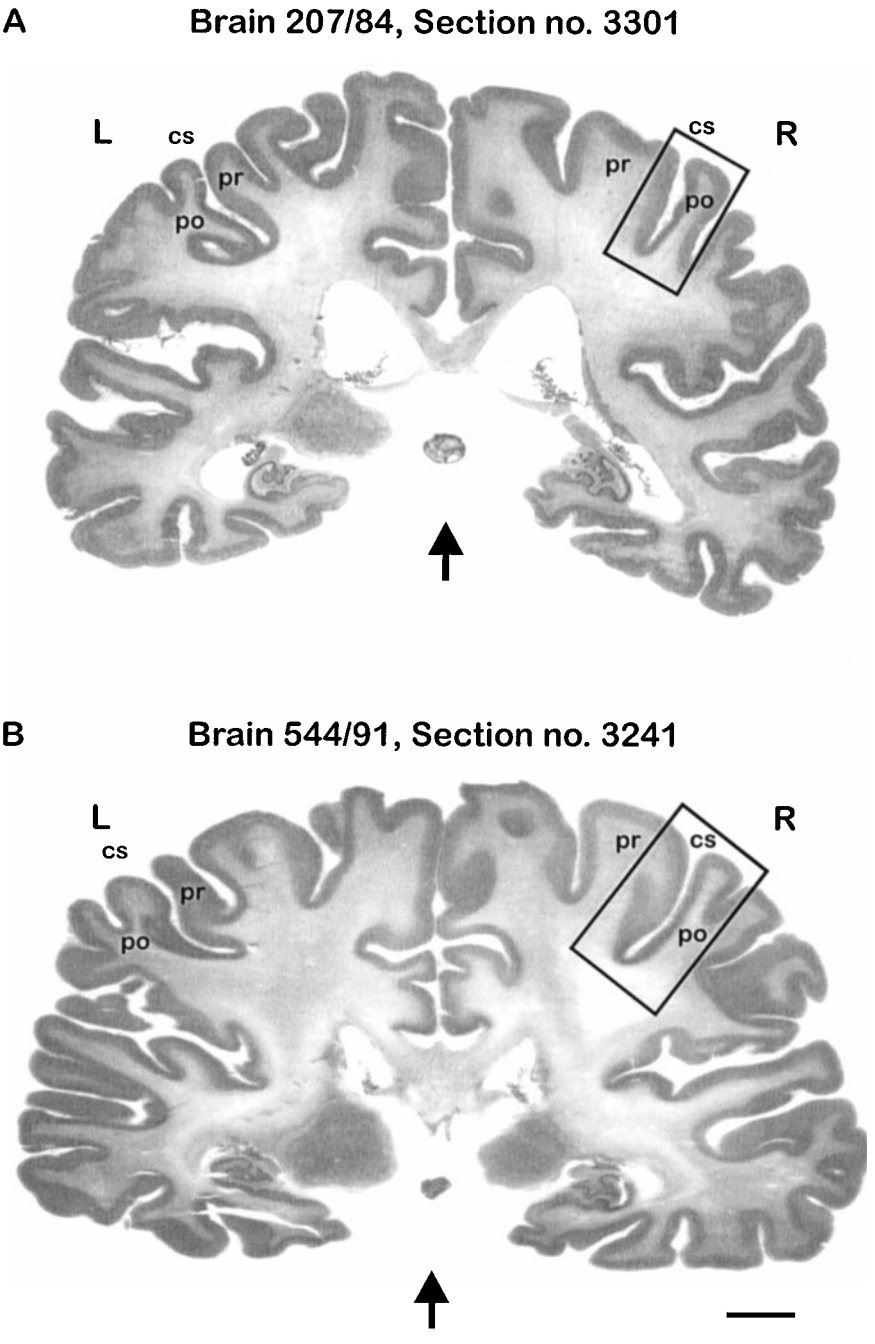

FIG. 1. Two cell-stained whole brain sections cut in the coronal plane from two different brains [brain 207/84, section 3301 (A), and brain 544/91, section 3241 (B)]. Boxes show regions of interest covering the caudal bank of the precentral gyrus (pr) and the rostral and caudal banks of the postcentral gyrus (po) which were used for GLI measurements and subsequent extraction of profiles. Note compression of each brain parallel to the direction of sectioning (arrows). L, left hemisphere; R, right hemisphere; cs, central sulcus. Bar, 10 mm.

(Fig. 1A), is shown at higher magnification in Fig. 2A. The cytoarchitectonic differences between primary motor cortex in the precentral and primary somatosensory cortex in the postcentral gyrus are already evident at this low spatial resolution: a wide band of gray matter, low cell density, and a blurred border between gray and white matter in the precentral gyrus versus a narrow band of gray matter, high cell density, and a sharp border between gray and white matter in the postcentral gyrus. The border (arrowhead) lies in the caudal bank of the precentral gyrus close to the fundus of the central sulcus. The corresponding GLI image is shown in Fig. 2B. It also shows these differences in cytoarchitecture between pre- and postcentral gyrus. Local variations in staining intensity of the background (asterisks in Fig. 2A), however, are absent in the GLI

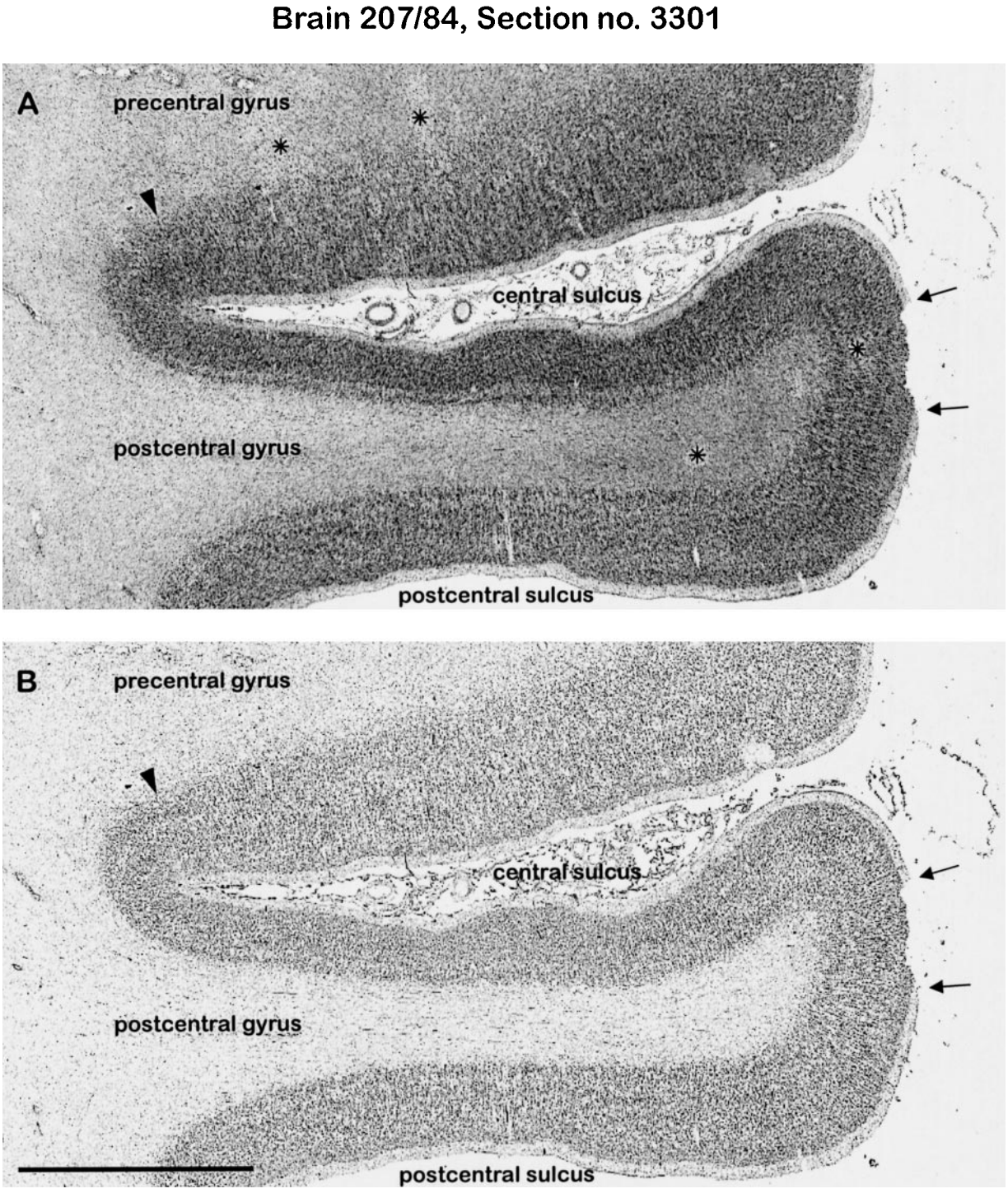

FIG. 2. Region of interest depicted in Fig. 1A shown at higher magnification. Cell-stained section (A) and corresponding GLI image (B) which was used for extraction of profiles. The GLI image was inverted prior to printing. Arrowheads mark the border between primary motor and primary somatosensory cortex. Arrows point to an artifact on the crown of the postcentral gyrus (layer I and partly layer II of the cortex are missing). Asterisks in A indicate local inhomogeneities in staining intensity of the background which are absent in the GLI image. Bar, 5 mm.

image due to the thresholding procedure. The GLI images were used for profile extraction and observer-independent detection of borders; the cell-stained sections were used for subsequent cytoarchitectonic classification.

Section 3361 (brain 207/84) is mapped in Fig. 3. Equidistant profiles 300 µm apart were extracted from position 1 in the caudal bank of the precentral gyrus to position 150 in the caudal wall of the postcentral gyrus (cf. Fig. 5C). In this set of profiles, the effect of increas-

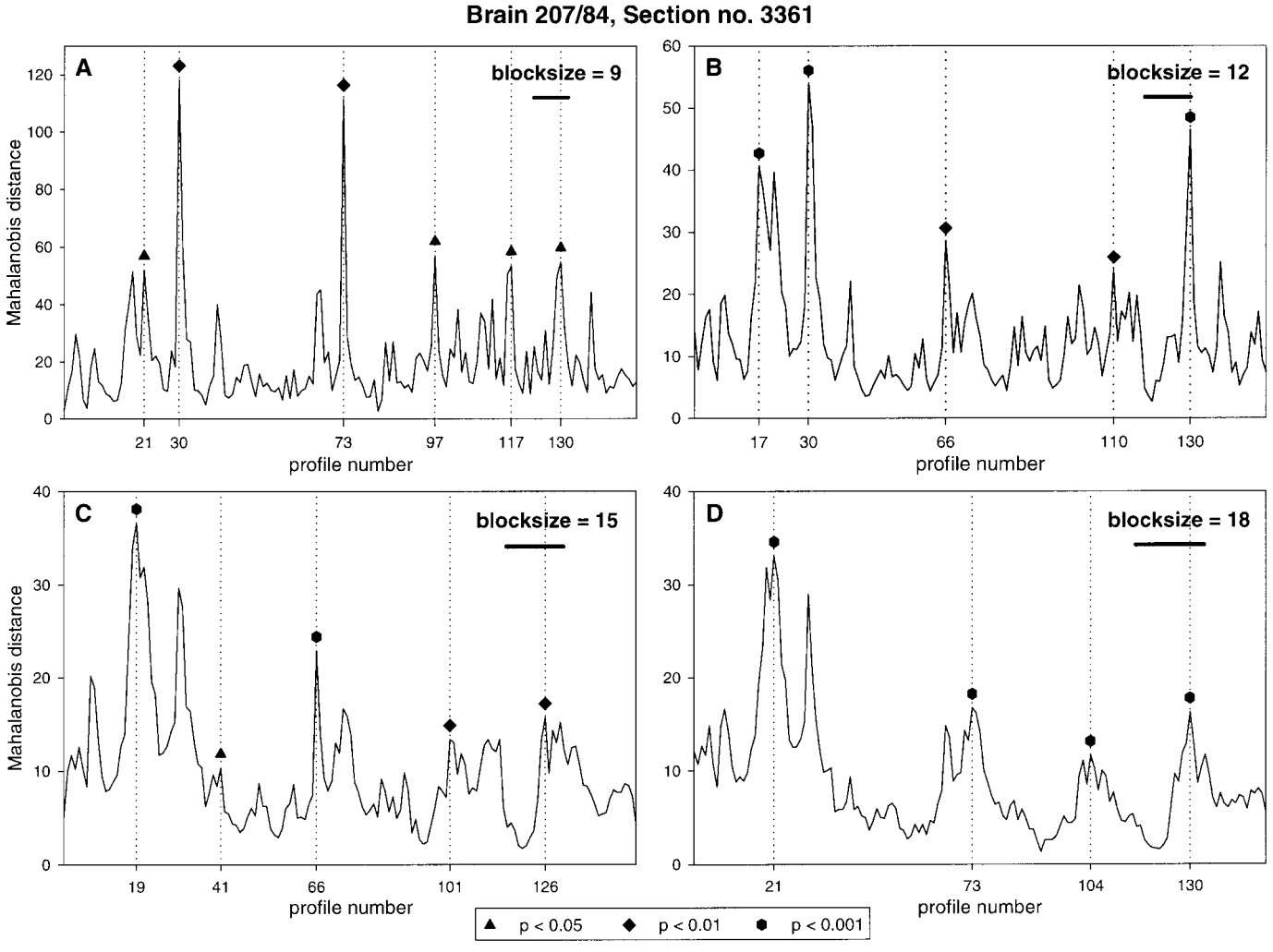

FIG. 3. One set of profiles (brain 207/84, section 3361) is processed for different numbers of adjacent profiles per block to show the effect of increasing values of b (smoothing effect): $b_1 = b_2 = 9$ (A), $b_1 = b_2 = 12$ (B), $b_1 = b_2 = 15$ (C), and $b_1 = b_2 = 18$ (D). Values of the Mahalanobis distance function (ordinate) are plotted against positions of the profile blocks relative to the cortex (abscissa). Main maxima are marked with dotted lines. Symbols indicate levels of significance. Bars indicate widths of one block of profiles which define the spatial resolution. See Materials and Methods for further details.

ing values of b (i.e., smoothing) is demonstrated by processing the same profiles for different numbers of adjacent profiles per block (b_1,b_2): $b_1 = b_2 = 9$ (Fig. 3A), $b_1 = b_2 = 12$ (Fig. 3B), $b_1 = b_2 = 15$ (Fig. 3C), and $b_1 = b_2 = 18$ (Fig. 3D). Main maxima are marked with dotted lines. Symbols indicate levels of significance. Note that the degree of smoothing increases with higher numbers of profiles per block. The positions of several main maxima, however, do not seem to be influenced by the block size being used: they can be reproduced at similar positions in the cortex. The maximum at position 21 in Fig. 3A seems to correspond to maxima 17 in Fig. 3B, 19 in Fig. 3C, and 21 in Fig. 3D. Additional corresponding maxima seem to be present at positions (in Figs. 3A to 3D) 73–66–66–73, 97–110–101–104, and 130–130–126–130. Positions of significant maxima are plotted against blocksizes from $b = 8$ to $b = 20$ in Fig. 4 (section 3361; Fig. 4C; dotted vertical line "A" corresponds to Fig. 3A, line "B" to Fig. 3B, etc.). With increasing b-values some main maxima are eliminated, but others can be reproduced at comparable positions across a wide range of block sizes especially toward higher b-values, i.e., the maxima at positions 21, 73, 104, and 130 (Fig. 4C). Comparable maxima can be found at similar positions in a series of nearby sections from the same brain (Fig. 4): in section 3421 (1.2 mm further rostral than section 3361; Fig. 4A) at positions 20, 85, 115, and 149 (cf. Fig. 5A); in section 3301 (1.2 mm further caudal than section 3361; Fig. 4E) at positions 20, 76, and 131 (cf. Fig. 5E); and in section 3241 (2.4 mm further caudal than section no. 3361; Fig. 4G) at positions 20, 78, 104, and 128 (cf. Fig. 5G).

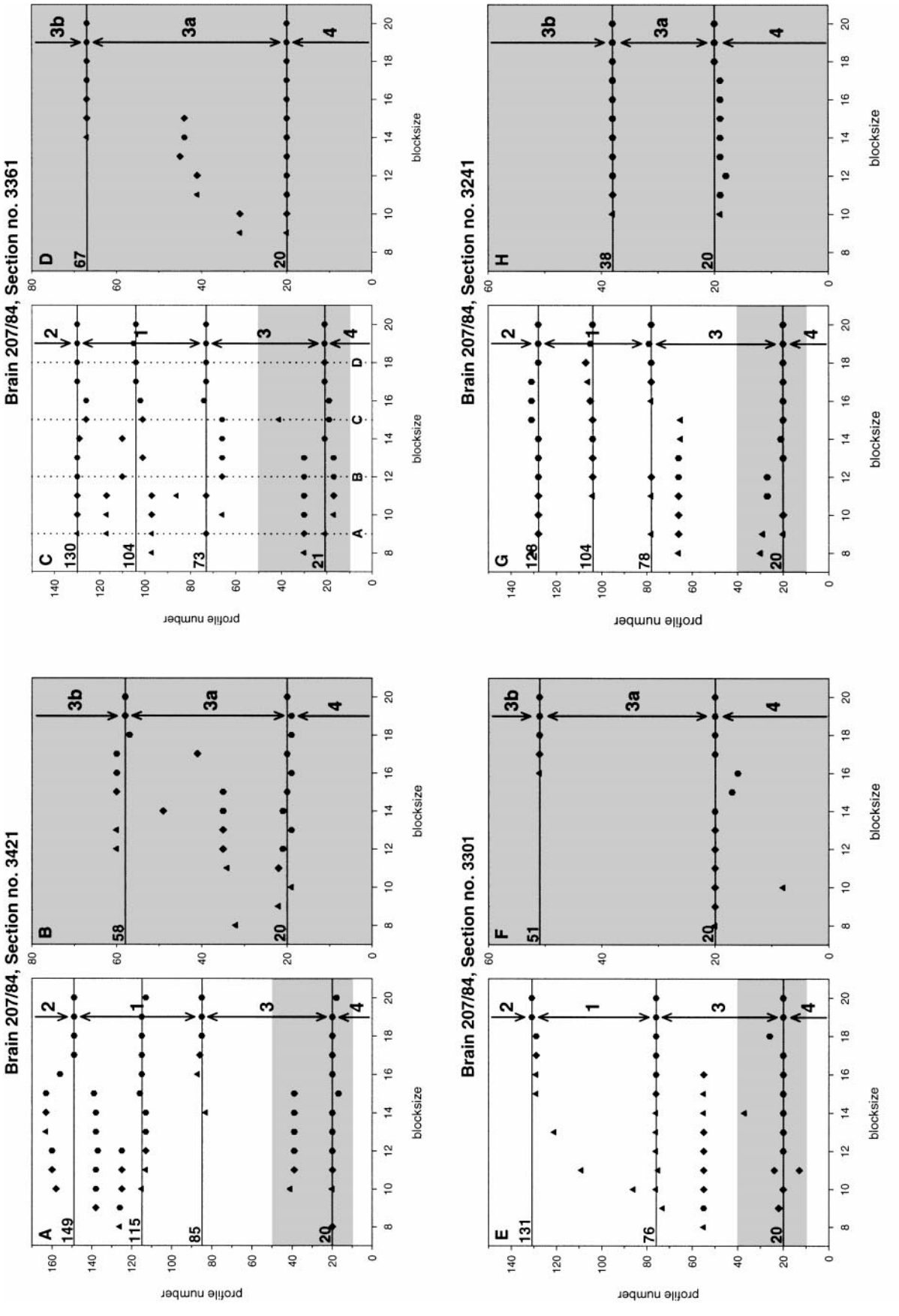

FIG. 4. Positions of significant maxima (ordinate) are plotted against block sizes (abscissa) in brain 207/84, sections 3421 (A, B), 3361 (C, D), 3301 (E, F), and 3241 (G, H). Low-resolution mode is shown in A, C, E, and G. Shaded regions were rescanned in high-resolution mode. Results are shown in B, D, F, and H, respectively. Dotted vertical line "A" in C corresponds to Fig. 3A; line "B" to Fig. 3B, etc. Same symbols as in Fig. 3. Arrows mark extent of areas 4, 3, 3a, 3b, 1, and 2.

The positions of these main maxima are compared with visible changes in cytoarchitecture in order to further elucidate the nature of the microstructural entities delineated by these borders. The maxima at positions 20 (Fig. 5A), 21 (Fig. 5C), 20 (Fig. 5E), and 20 (Fig. 5G) lie in the caudal bank of the precentral gyrus close to the fundus of the central sulcus. The cytoarchitectonic pattern in this region (Fig. 6A) reveals a wide band of gray matter, low cell density, a pronounced columnar arrangement of the cells, and a blurred border between gray and white matter in the precentral gyrus (left) versus a narrow band of gray matter, high cell density, an incipient layer IV, and a sharp border between gray and white matter in the postcentral gyrus (right). The position of the border between primary motor area 4 and primary somatosensory area 3 is marked and matches very closely the corresponding borders defined in an objective way. The maxima at positions 85 (Fig. 5A), 73 (Fig. 5C), 76 (Fig. 5E), and 78 (Fig. 5G) lie in the superficial part of the rostral bank of the postcentral gyrus. The cytoarchitectonic pattern in this region (Fig. 7A) shows typical granular cortex with high cell density (left) versus lower cell density, a more pronounced columnar arrangement of the cells, and fairly large and elongated pyramidal cells in lower layer III (right). The position of the border between primary somatosensory areas 3 and 1 is marked and again matches very closely the corresponding borders defined objectively. Maxima 115 (Fig. 5A), 104 (Fig. 5C), and 104 (Fig. 5G) lie at comparable positions on the crown of the postcentral gyrus. Subjective analysis reveals no visible change in cytoarchitecture at this position. Maxima 149 (Fig. 5A), 130 (Fig. 5C), 131 (Fig. 5E), and 128 (Fig. 5G) lie at comparable positions in the caudal bank of the postcentral gyrus. The cytoarchitectonic pattern in this region (Fig. 7B) again shows fairly large and elongated lower layer III pyramids which are characteristic of area 1 (right) versus slightly lower cell density and much smaller lower layer III pyramids (left). The position of the border between areas 1 and 2 is marked and again matches very closely the corresponding borders defined in an observer-independent way.

According to the literature, area 3 can be further subdivided into areas 3a and 3b. The algorithm did not detect any subdivisions within area 3 which might suggest the existence of areas 3a or 3b. However, the spatial extent of area 3a is very small (it lies in the fundus of the central sulcus), and the spatial resolution of the algorithm is governed not only by the block size being used but also by the distance (in μm) between adjacent profiles. For this reason, a ROI covering the fundal region of the central sulcus in each section (shaded regions in Figs. 4A, 4C, 4E, and 4G) was rescanned with higher spatial resolution (i.e., equidistant profiles were extracted 150 μm apart instead of 300 μm). Results are shown in Figs. 4B, 4D, 4F, and 4H, respectively. The maxima at positions 20 (Figs. 5B, 5D, 5F, and 5H) lie in the caudal bank of the precentral gyrus close to the fundus of the central sulcus and correspond to the border between area 4 and area 3. The maxima at positions 58 (Fig. 5B), 67 (Fig. 5D), 51 (Fig. 5F), and 38 (Fig. 5H) lie at comparable positions in the postcentral gyrus close to the fundus of the central sulcus. The cytoarchitectonic pattern in this region (Fig. 6B) shows granular cortex with somewhat lower cell density, a more pronounced columnar arrangement of the cells, and medium-sized pyramids scattered throughout lower layer III and layer V (left) versus high cell density, no columnar arrangement, and absent medium-sized pyramids (right). The position of the border between areas 3a and 3b is marked and matches very closely the corresponding borders defined objectively.

Figures 8–11 show the degree of interindividual variability of areas 3a, 3b, and 1 and their correlation with macroscopical landmarks (i.e., gyri and sulci) in eight different brains. One coronal section per brain from a comparable rostrocaudal level was scanned in the same way as described above, i.e., the caudal bank of the precentral and the postcentral gyrus with equidistant profiles 300 μm apart and in addition a ROI covering the fundus of the central sulcus with equidistant profiles 150 μm apart. Positions of significant maxima are plotted against blocksizes in Figs. 8 and 10. Shaded regions in Figs. 8A, 8C, 8E, 8G, 10A, 10C, 10E, and 10G indicate ROIs which were rescanned with equidistant profiles 150 μm apart (results are shown in Figs. 8B, 8D, 8F, 8H, 10B, 10D, 10F, and 10H). Again, some main maxima are eliminated with increasing values of *b*, but others can be reproduced at comparable positions across a wide range of block sizes. Their positions closely match the cytoarchitectonic transitions between areas 4/3a, 3a/3b, 3b/1, and 1/2 as shown in Figs. 6 and 7. At some positions, however, visual analysis reveals no appreciable change in the cytoarchitectonic pattern. The resulting areal maps are shown in Figs. 9 and 11. At position 41 in brain 382/81, section 3751 (Fig. 11E), and position 42 in brain 56/94, section 3361 (Fig. 11G), borders are detected in low-resolution mode (i.e., equidistant profiles 300 μm apart) which can be reproduced at corresponding positions in high-resolution mode (i.e., equidistant profiles 150 μm apart; cf. Figs. 11F and 11H, respectively) and which, upon visual inspection, closely match the cytoarchitectonic transition between areas 3a and 3b as shown in Fig. 6B. Note that the spatial extent of area 3a parallel to the cortical layers is maximal in these two brains [in high-resolution mode between positions 19 and 67 = 48 profiles in brain 382/81 (Fig. 11F) and between positions 20 and 70 = 50 profiles in brain 56/94 (Fig. 11H)].

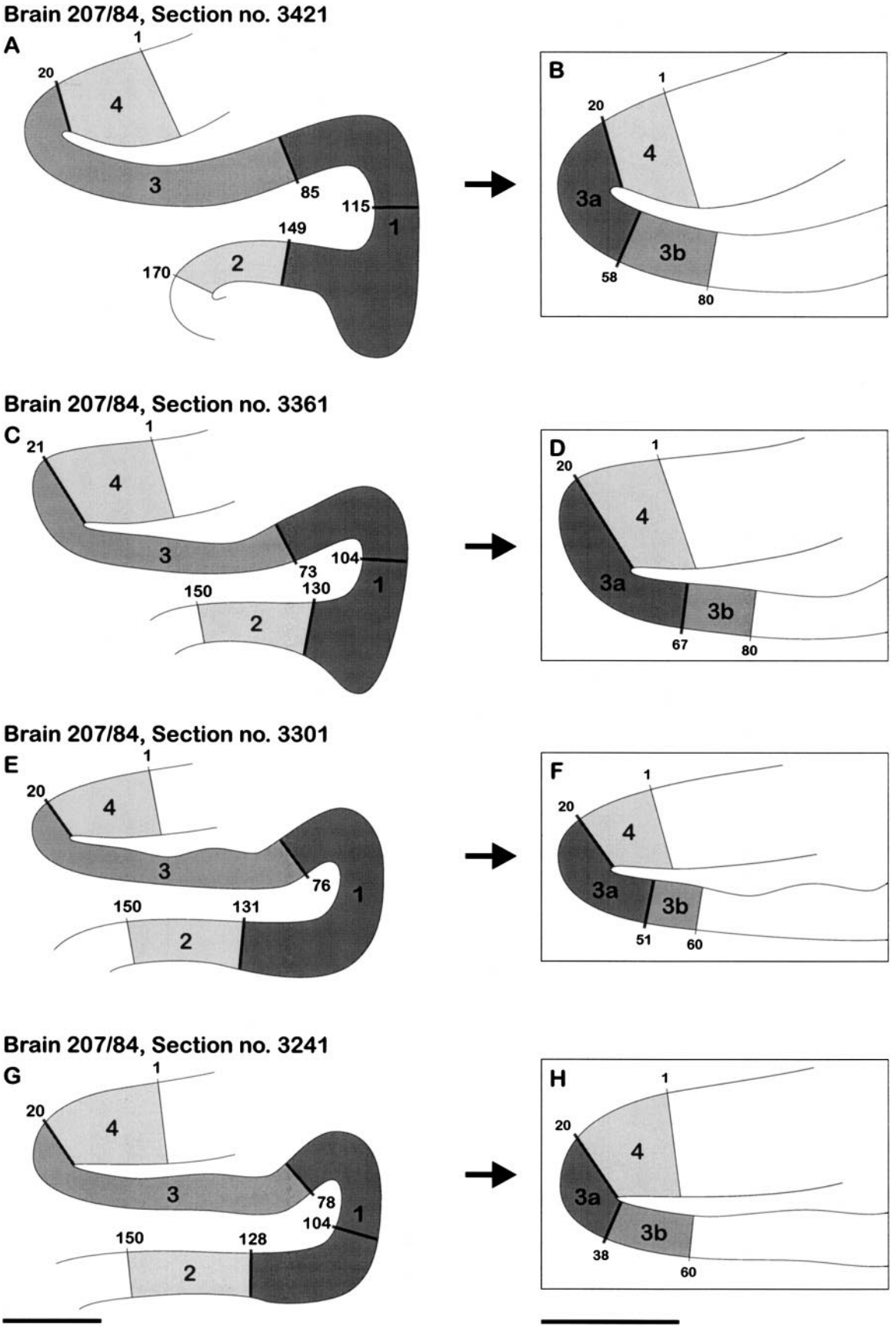

FIG. 5. Positions of borders and extent of areas 4, 3, 3a, 3b, 1, and 2 in brain 207/84, sections 3421 (A, B), 3361 (C, D), 3301 (E, F), and 3241 (G, H). Same sections as in Fig. 4. Low-resolution mode is shown in A, C, E, and G. ROIs covering the fundus of the central sulcus were rescanned in high-resolution mode. Results are shown in B, D, F, and H, respectively. Bars, 5 mm.

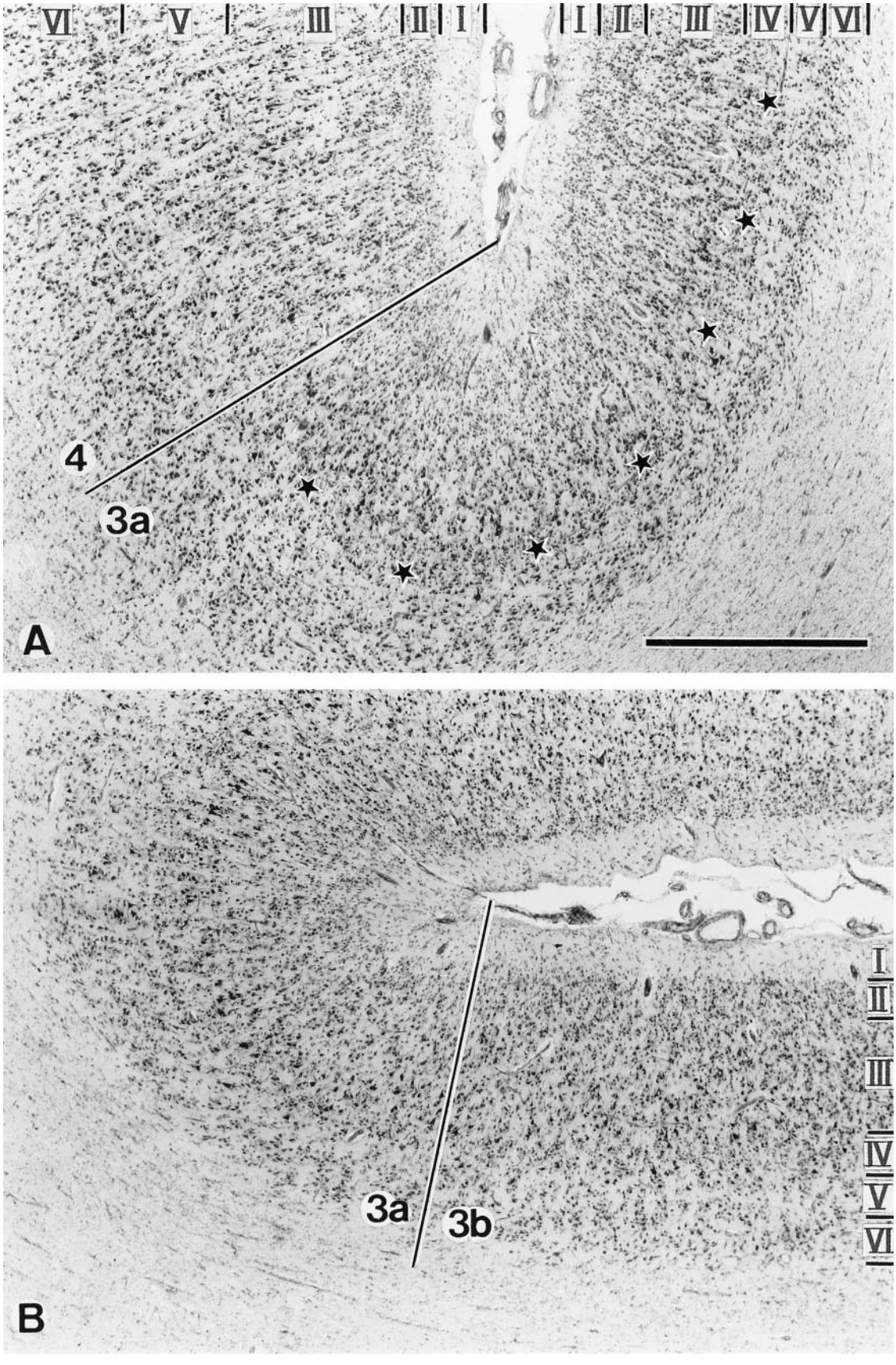

FIG. 6. Cytoarchitectonic features of the transitions between areas 4 and 3a (A) and between areas 3a and 3b (B). Both transitions are located close to the fundus of the central sulcus. Asterisks in A indicate incipient layer IV in area 3a. Roman numerals indicate cortical layers. Bar, 1 mm.

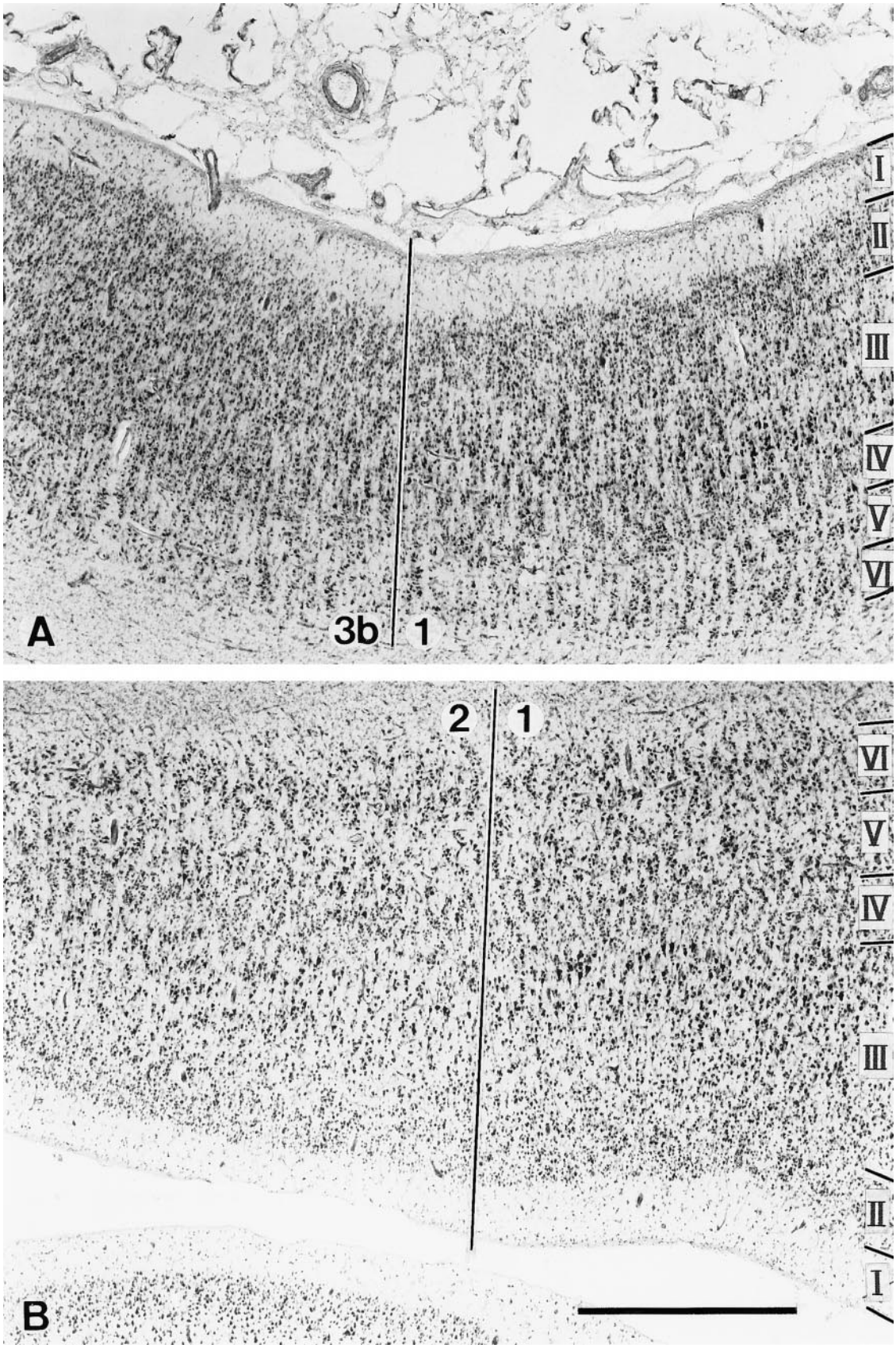

FIG. 7. Cytoarchitectonic features of the transitions between areas 3b and 1 in the rostral bank (A) and between areas 1 and 2 in the caudal bank of the postcentral gyrus (B). Roman numerals indicate cortical layers. Bar, 1 mm.

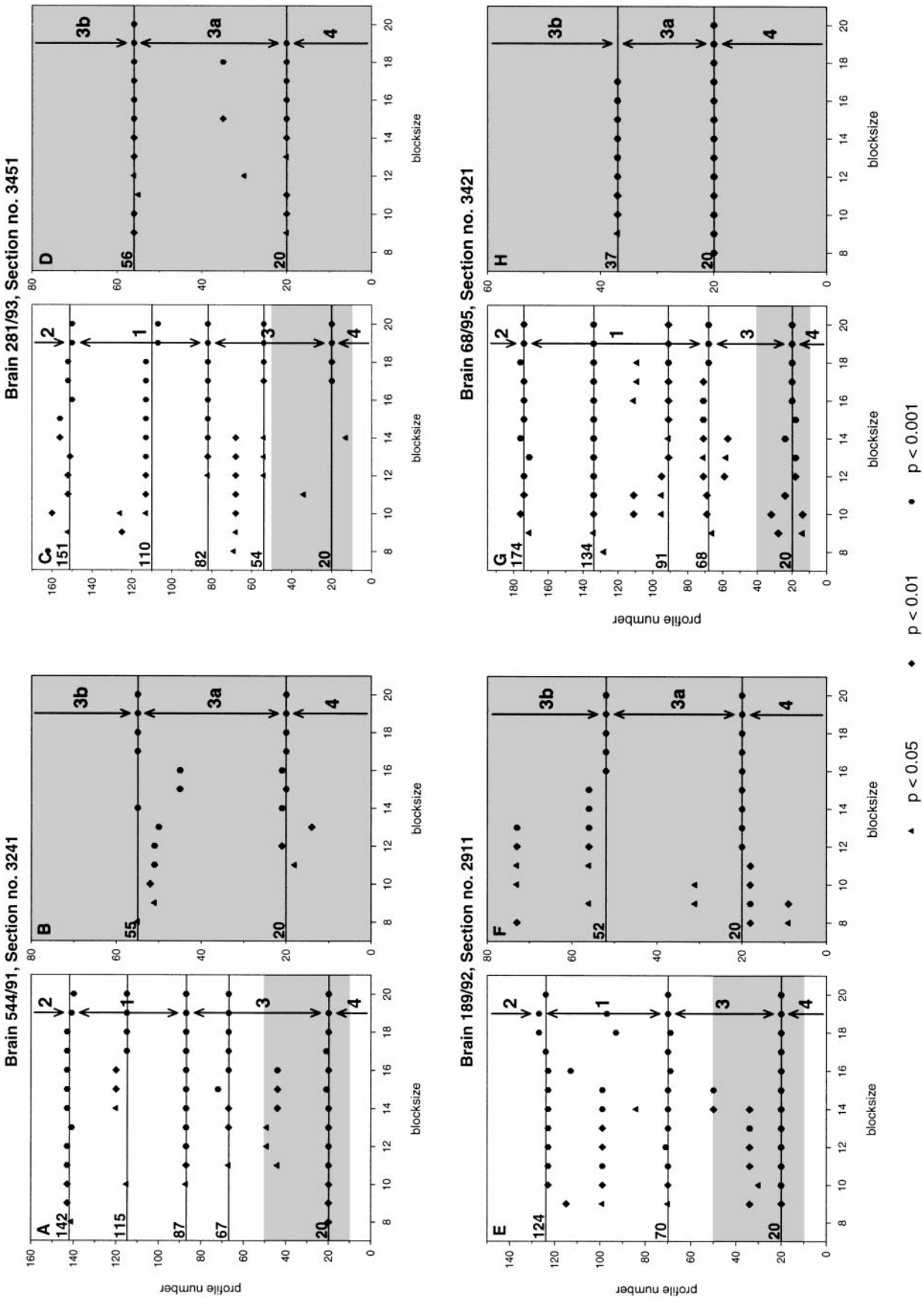

FIG. 8. Positions of significant maxima (ordinate) are plotted against block sizes (abscissa) in brain 544/91, section 3241 (A, B); brain 281/93, section 3451 (C, D); brain 189/92, section 2911 (E, F); and brain 68/95, section 3421 (G, H). For other conventions see Fig. 4.

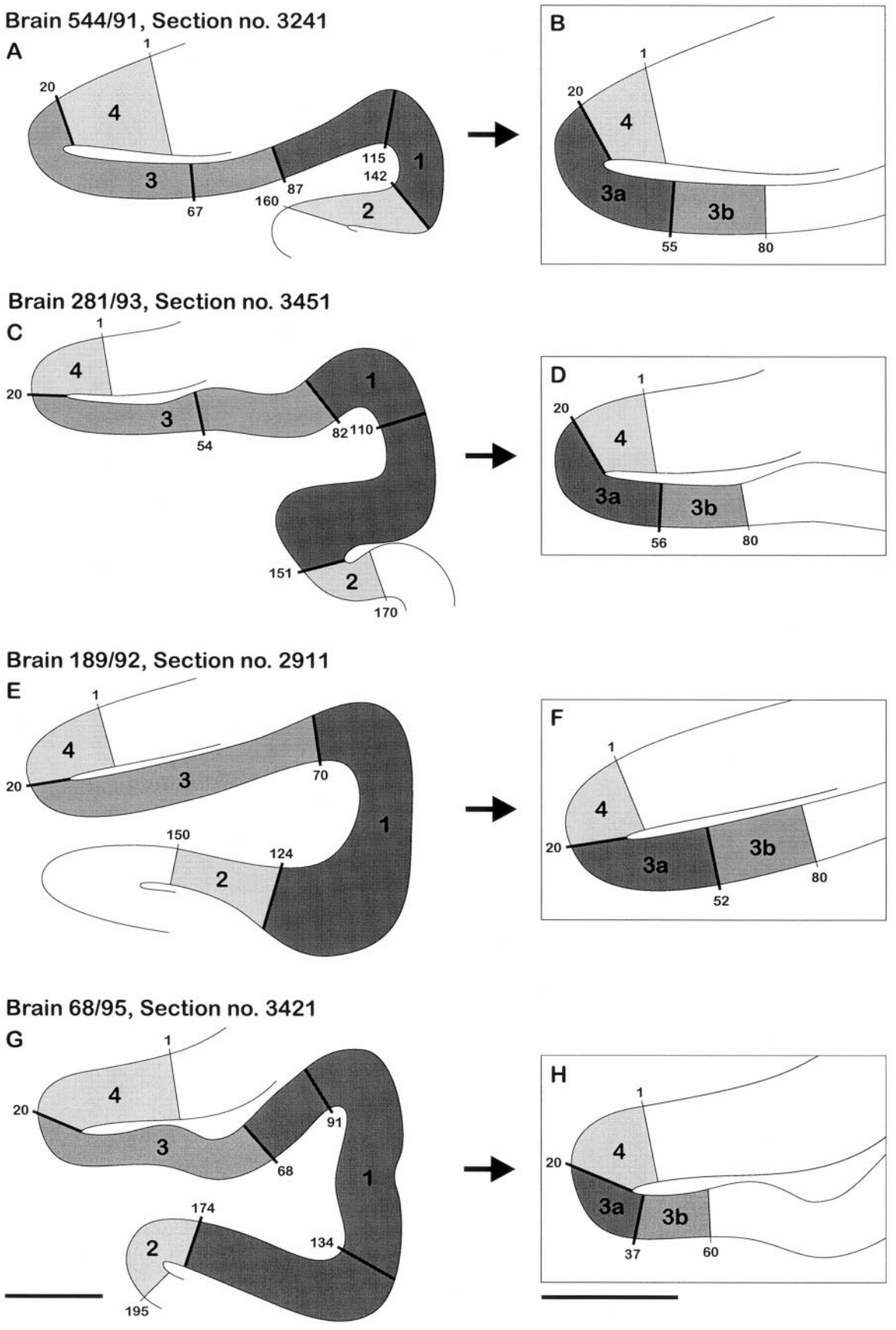

FIG. 9. Positions of borders and extent of areas 4, 3, 3a, 3b, 1, and 2 in brain 544/91, section 3241 (A, B); brain 281/93, section 3451 (C, D); brain 189/92, section 2911 (E, F); and brain 68/95, section 3421 (G, H). Same brains and sections as in Fig. 8. For other conventions see Fig. 5. Bars, 5 mm.

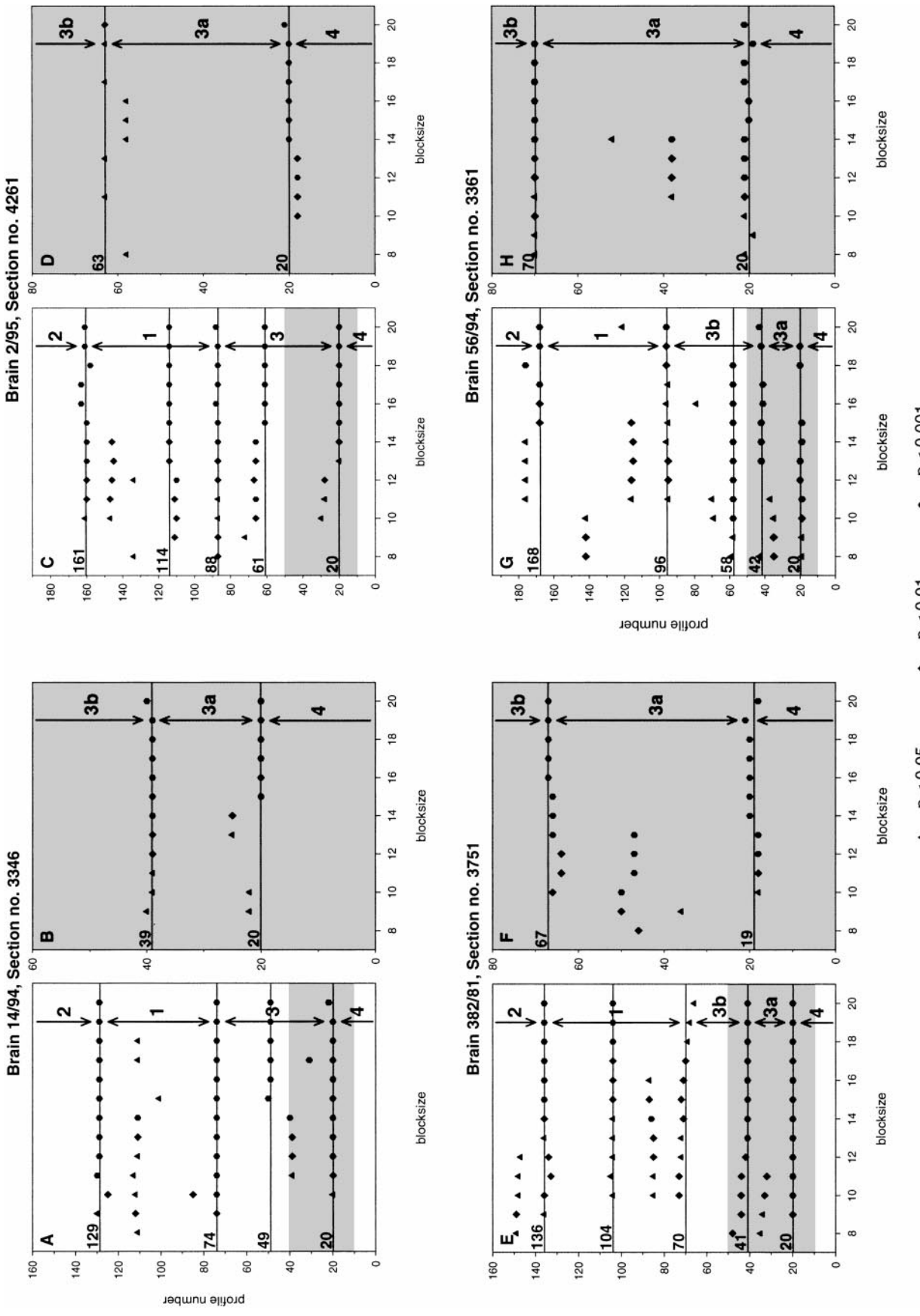

FIG. 10. Positions of significant maxima (ordinate) are plotted against block sizes (abscissa) in brain 14/94, section 3346 (A, B); brain 2/95, section 4261 (C, D); brain 382/81, section 3751 (E, F); and brain 56/94, section 3361 (G, H). For other conventions see Fig. 4.

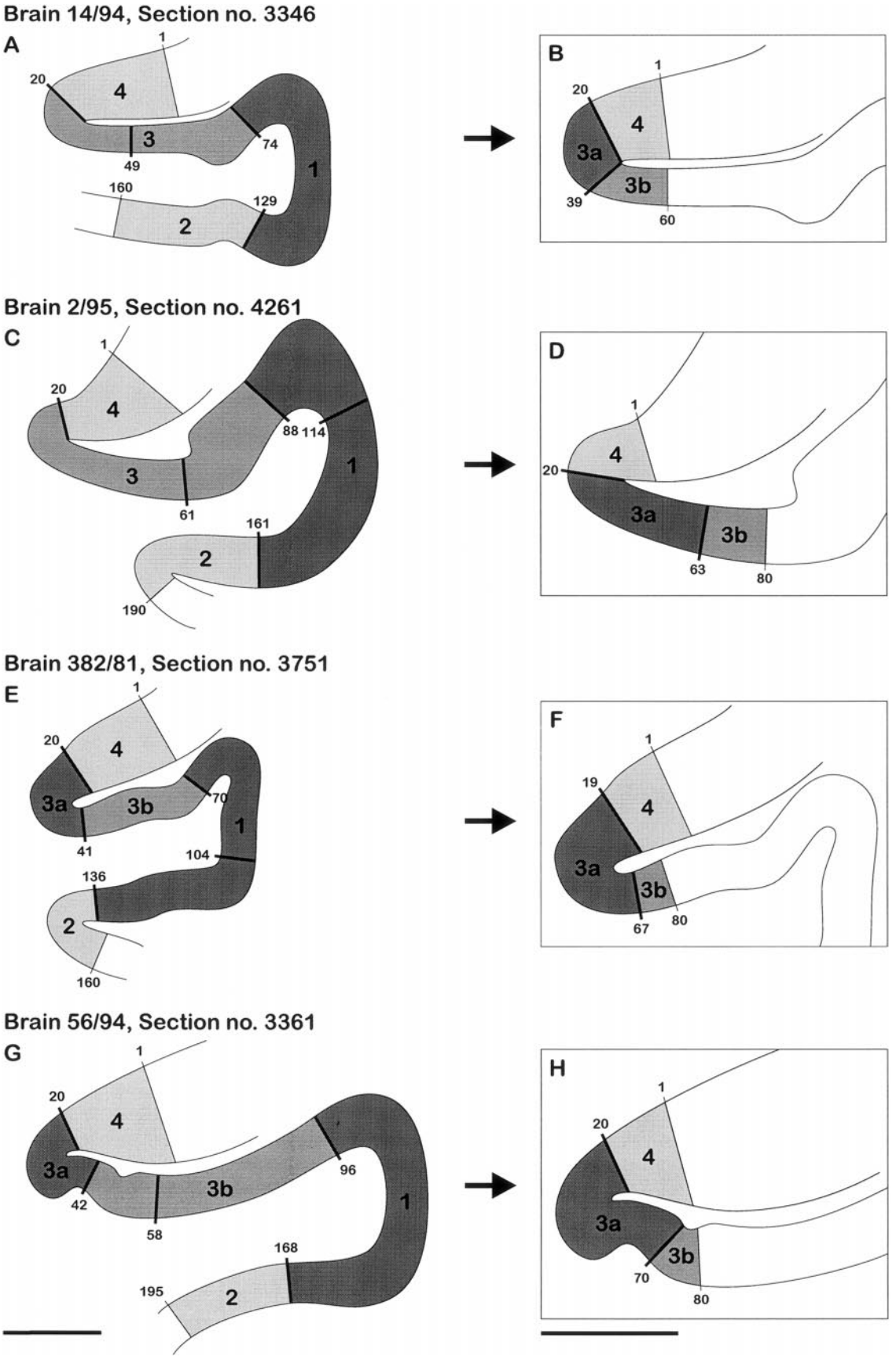

FIG. 11. Positions of borders and extent of areas 4, 3, 3a, 3b, 1, and 2 in brain 14/94, section 3346 (A, B); brain 2/95, section 4261 (C, D); brain 382/81, section 3751 (E, F); and brain 56/94, section 3361 (G, H). Same brains and sections as in Fig. 10. For other conventions see Fig. 5. Bars, 5 mm.

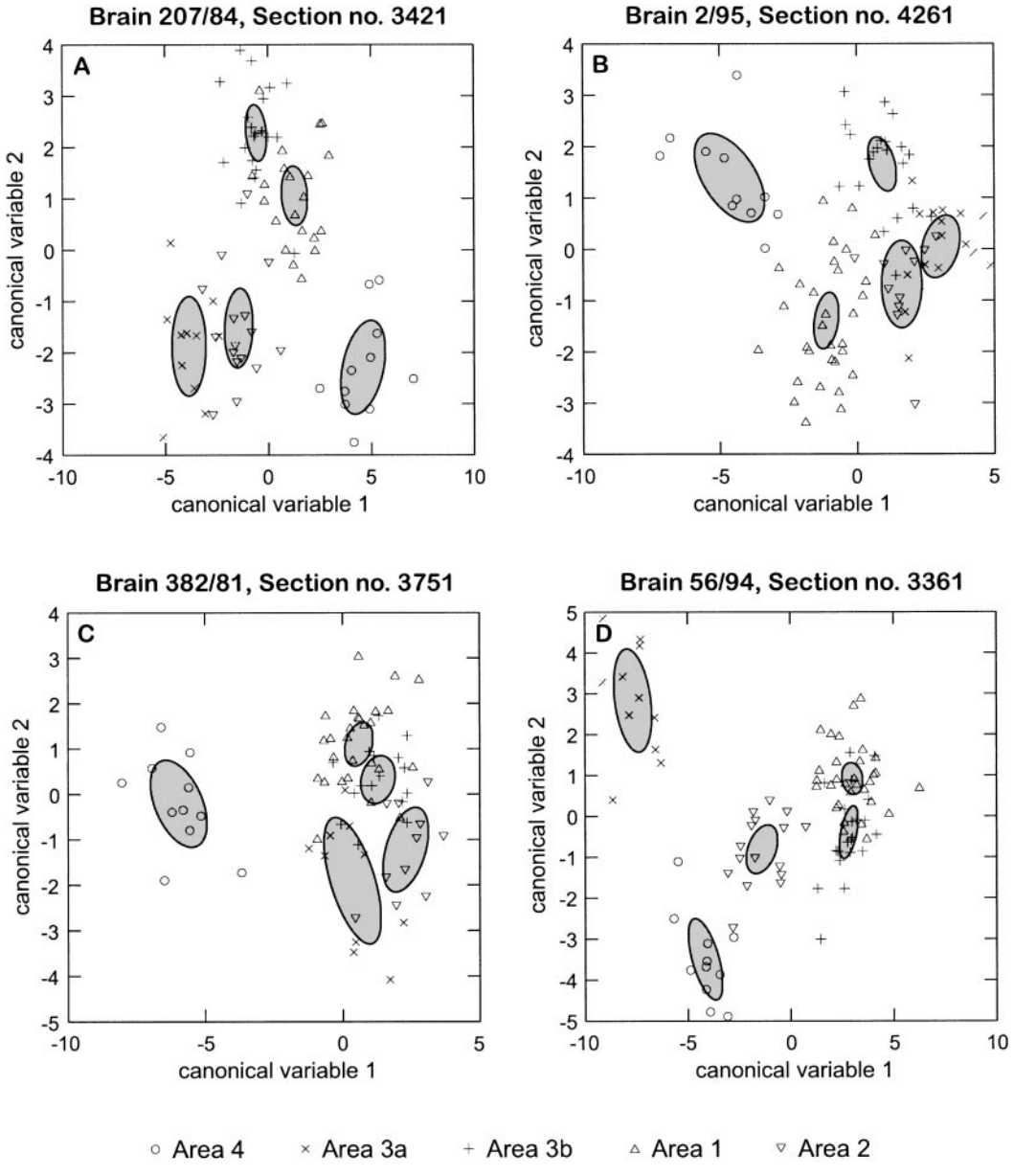

FIG. 12. Discriminant analysis of profiles sampled from areas 4, 3a, 3b, 1, and 2 in four different brains (one section per brain): brain 207/84, section 3421 (A); brain 2/95, section 4261 (B); brain 382/81, section 3751 (C); and brain 56/94, section 3361 (D). Open symbols represent single profiles; shaded regions represent 95% confidence areas of each group's centroid.

All the profiles sampled in low-resolution mode from one section were grouped into five classes (i.e., belonging to areas 4, 3a, 3b, 1, or 2) based on this definition of interareal borders. A discriminant analysis was then performed for each section. The result of each analysis is graphically presented by using the first two canonical variables (Fig. 12). Four different brains are shown, one section per brain. In the sections from brains 207/84 and 2/95 (Figs. 12A and 12B), area 3a is too small to be detected in low-resolution mode (cf. Figs. 5A and 11C). In the sections from brains 382/81 and 56/94 (Figs. 12C and 12D), area 3a is large enough to be detected in low-resolution mode (cf. Figs. 11E and 11G). Symbols represent single profiles; shaded regions represent 95% confidence areas of each group's centroid. In each section, differences in profile shapes between the five cortical areas result in clusters without any overlap among the 95% confidence areas.

All ROIs shown were sampled from right hemispheres and from comparable rostrocaudal levels. Two findings are obvious in all brains: Cytoarchitectonic interareal borders do not match macrostructural landmarks of the postcentral gyrus, and they vary considerably in their positions relative to these landmarks across different brains.

DISCUSSION

In this study we mapped human primary somatosensory areas 3a, 3b, and 1 by using a combination of objective and observer-independent delineation of cytoarchitectonic borders followed by cytoarchitectonic classification. Cytoarchitectonic mapping of the human somatosensory cortex has been done several times in the past (Campbell, 1905; Brodmann, 1909; von Economo and Koskinas, 1925; Bailey and von Bonin, 1951; Sarkissov *et al.*, 1955; White *et al.*, 1997). Our mapping approach, however, is new in so far as *cytoarchitectonic borders can be defined in an objective way.* This obviates subjective evaluation of differences in the cytoarchitectonic pattern (and all problems related to it) which has so far been the only way to structurally define cortical areas. As a second step, it is necessary to *interpret and classify these cytoarchitectonic entities* which implies a certain degree of subjectivity, e.g., when correlating the cytoarchitectonic features of these entities with verbal or pictorial descriptions published in the literature.

Hence, the whole procedure implies two steps: (i) objective definition of cytoarchitectonic borders, followed by (ii) interpretation and classification of the cytoarchitectonic entities surrounded by these borders.

Objective Definition of Cytoarchitectonic Borders

The approach is based on the assumption that microstructural entities of the cerebral cortex are characterized by a specific cytoarchitectonic pattern which differs from that of neighboring entities. Density profiles extracted perpendicularly to the pial surface across cortical layers II–VI quantify this cytoarchitectonic pattern. Maximum differences in profile shapes can be expected when two groups of profiles sampled from two different entities are compared. Although each profile is 125 μm wide, single profiles are affected by local structural inhomogeneities, e.g., cell clusters or blood vessels. Thus, in order to smooth the signal, and improve the signal-to-noise ratio of the distance function, two adjacent groups of profiles were compared instead of two adjacent single profiles (see also Schleicher *et al.*, 1999).

Many main maxima of the Mahalanobis distance function are fairly sharp peaks, especially toward smaller block sizes (cf. Fig. 3). This, however, should not be interpreted as an emerging renaissance of the Vogts' discussions on "haarscharfe Grenzen" (i.e., boundaries as sharp or fine as a hair). The photographs show that there is always a more or less wide transition zone around a cytoarchitectonic border in which the cytoarchitectonic pattern of one entity merges into the pattern of the adjacent entity. Main maxima define that point in each transition zone where the degree of cytoarchitectonic dissimilarity between the two entities is maximal (see also Schleicher *et al.*, 1999).

Other factors may also influence the shapes of profiles and may be responsible for additional significant maxima. Variations in staining intensity of cell bodies or background within a section, across different sections, and across different brains are a critical issue. This problem, however, is irrelevant in our study because the profiles were extracted not from digitized images of the cell-stained sections but instead from GLI images in which cell bodies have been segmented from the background by adaptive thresholding (Schleicher and Zilles, 1990; cf. Fig. 2A with 2B in which local variations in staining intensity of the background, marked with asterisks in Fig. 2A, are absent). Artifacts due to sectioning of the tissue (e.g., tears) are a major problem when analyzing large or even whole brain sections as was done in this study. However, one should keep in mind that the number of profiles per block (b_1, b_2) limits the spatial resolution of the algorithm (from $b = 8 \times 300$ μm $= 2.4$ mm to $b = 20 \times 300$ μm $= 6$ mm in low-resolution mode or from 1.2 to 3 mm in high-resolution mode). Only entities wider than a cortical sector covered by one block of profiles can be resolved with correct distance values. Small artifacts are irrelevant. As soon as their length parallel to the cortical layers exceeds the threshold of spatial resolution, they are a potential source of false-positive borders. The artifact on the crown of the postcentral gyrus shown in Figs. 2A and 2B (arrows) measures around 2.5 mm parallel to the cortical layers and lies approximately at the threshold of spatial resolution for small values of b (low-resolution mode). In addition, artifacts are usually distributed randomly throughout the cortex, and this should become evident when comparing a series of consecutive sections. Cortical arteries and veins rarely exceed 200 μm in diameter and they are oriented more or less perpendicularly to the cortical layers. Smaller vessels arise from the principal trunk and spread out at different angles but their length parallel to the cortical layers does not reach the threshold of spatial resolution (Duvernoy *et al.*, 1981). Cortical columns or modules are a basic structural and functional principle of the cerebral cortex. In the somatosensory cortex, each column is 300–400 μm wide and contains approximately 80 minicolumns of 50–60 μm in diameter (Mountcastle, 1997). Hence, cortical columns and minicolumns do not reach the threshold of spatial resolution. In gyrencephalic brains, inward and outward folds of the cortex cause distortions of the cytoarchitectonic pattern (cf., e.g., Van Essen, 1997). In order to assess to what extent cortical folding causes false-positive borders, a model of a layered cortical region was generated (Schleicher *et al.*, 1999). In this study, five layers were represented by horizontal stripes with different GLI values, and random noise was added. Interareal bor-

ders were predefined at several positions by introducing step-like changes in GLI values oriented perpendicularly to the stripes. In addition, a low frequency sine-shaped thinning of layer II was inserted which represents a distortion in the thickness of layers II and III induced by cortical folding. The distance function detected all borders with sharp and significant maxima but not the sine-shaped distortion (Schleicher *et al.*, 1999). In addition, Figs. 5, 9, and 11 of the present study show that those positions at which the curvature of the cortex is maximal (e.g., fundi of sulci) do not coincide with positions of main maxima.

Interpretation and Classification of the Cytoarchitectonic Entities Surrounded by These Borders

The next step is to interpret and classify the cytoarchitectonic entities surrounded by these borders. The positions of several borders closely match transitions in the cytoarchitectonic pattern which are readily visible. The first complete cytoarchitectonic map of the human brain by Campbell (1905) defined only two areas in the postcentral gyrus, a "postcentral" and an "intermediate postcentral" area. The former occupies mainly the rostral half, and the latter the caudal half of the postcentral gyrus. The most famous cytoarchitectonic map, still widely used today, is the map of Brodmann. He described one area in the caudal wall of the precentral gyrus (area 4) and three areas in the postcentral gyrus (area 3 in the rostral wall, area 1 on the crown, and area 2 in the caudal wall). Unfortunately, Brodmann's publications (1903, 1908, 1909) are not very helpful as they do not contain detailed morphological descriptions of the areas and also lack photographic illustrations. He only briefly comments on the topographic localization of each area, and the map is just a sketch showing each area's extent on the free cortical surface only. In addition to areas 3, 1, and 2, Brodmann described a small transition zone in the rostral part of area 3, located in the fundus of the central sulcus, and characterized by scattered large pyramidal cells and an internal granular layer. Later, Vogt and Vogt (1919) termed this region "area 3a." In contrast to Brodmann, von Economo and Koskinas (1925) meticulously described each area's cytoarchitectonic features and also included photomicrographs. They delineated one area in the caudal wall of the precentral gyrus: area FA, being characterized by low cell density, absent layer IV, and giant pyramidal cells in layer V. Area FA seems to correspond to Brodmann's area 4. Four areas were defined in the postcentral gyrus: areas PA, PB, PC, and PD. An emerging layer IV and medium-sized pyramids in lower layer III and layer V characterize area PA which lies in the fundus of the central sulcus. Most probably, it corresponds to area 3a of Brodmann and Vogt and Vogt. Area PB lies in the rostral wall of the postcentral gyrus and is characterized by high cell density across layers II–VI. Medium to large pyramids in layers III and V are missing. It seems to correspond to area 3b of Brodmann and Vogt and Vogt. Area PC occupies the crown of the postcentral gyrus and is characterized by large pyramidal cells in lower layer III. It seems to correspond to Brodmann's area 1. Area PD lies in the caudal wall of the postcentral gyrus. The prominent band of lower layer III pyramids is missing. Area PD most probably corresponds to Brodmann's area 2. Bailey and von Bonin (1951) defined only two regions in the postcentral gyrus: a band lying in the rostral wall which they termed "koniocortex" and "parakoniocortex" occupying crown and caudal wall of the gyrus. The last complete cytoarchitectonic map of the human cortex by Sarkissov and co-workers (1955) is to some extent a synopsis of Brodmann's and the Vogt and Vogt's work. Similar to Brodmann, they delineated three areas: area 3 in the rostral wall, area 1 on the crown, and area 2 in the caudal wall of the postcentral gyrus. A recent cytoarchitectonic study of the primary sensorimotor cortex (White *et al.*, 1997) adopted the Brodmann/Vogt nomenclature and mapped areas 3a, 3b, and 1. Extent and cytoarchitectonic features of area 3a match those of area PA according to von Economo and Koskinas (1925); area 3b corresponds to area PB, and area 1 to area PC.

In our sample of sections, low cell density and an absent layer IV can be found in the caudal bank of the precentral gyrus. Size and packing density of the giant pyramidal or Betz cells greatly varies across human brains (unpublished observations). They are fairly small and inconspicuous in the photograph shown here (cf. Fig. 6A). These features disappear around profile 20 in section 3421, brain 207/84 (Fig. 5A), and at corresponding positions in nearby sections. This corresponds to area 4. The prominent band of lower layer III pyramids emerges around profile 85 (same section) and disappears around profile 149. The entity in between is most likely area 1. Further caudally, lower layer III pyramids are much smaller. Cytoarchitecture and topography classify the entity caudal from profile 149 as, most probably, area 2. High cell density and layer IV classify the entity between profiles 20 and 85 as area 3.

According to the literature (see above), area 3 can be further subdivided into areas 3a and 3b. In some brains (e.g., 207/84 or 189/92) the algorithm (in low-resolution mode) did not detect any subdivisions within area 3 which might suggest the existence of areas 3a or 3b. In some other brains (e.g., 544/91 or 281/93) the algorithm (in low-resolution mode) detected borders approximately in the middle of area 3. Could this be the border between areas 3a and 3b? Several lines of evidence suggest that this is probably not so. First, an area 3a-like cytoarchitectonic entity has so far been described several times by different investigators in different brains and across the whole dorsomedial-to-ventrolateral extent of the central sulcus. Corresponding

borders should be present in all brains. Second, most investigators described area 3a as a small area lying in the fundus of the central sulcus, and they put the area 3a/3b border not far away from the fundus in the ascending part of the postcentral gyrus. The borders approximately in the middle of area 3 would suggest an unusually large extent of area 3a. Third, there are visible cytoarchitectonic differences between areas 3a and 3b (see above). However, no visible changes in cytoarchitecture are obvious at these borders in the middle of area 3. The most probable explanation that area 3a has been missed in low-resolution mode in most brains is indeed the small spatial extent of area 3a. An entity as small as area 3a in its classical description (see above) may easily escape detection, especially toward larger block sizes. However, the spatial resolution of the algorithm is governed not only by the block size being used but also by the distance (in μm) between adjacent profiles. For this reason, a ROI covering the fundal region of the central sulcus was rescanned with higher spatial resolution (i.e., equidistant profiles 150 μm apart instead of 300 μm). This procedure reliably detected borders within area 3 not far away from the fundus of the central sulcus in the ascending part of the postcentral gyrus in all brains. In addition, visible changes in cytoarchitecture are obvious at these borders (cf. Fig. 6B) which correspond to the transition between areas 3a and 3b published in the literature (see above). If the spatial extent of area 3a parallel to the cortical layers exceeds a certain threshold, the 3a/3b border can also be detected in low-resolution mode (and confirmed in high-resolution mode; cf. brains 382/81 and 56/94). In any case, a discriminant analysis based on this definition of the borders between areas 4, 3a, 3b, 1, and 2 confirmed this classification: five clusters of profiles were obtained without any overlap among the 95% confidence areas.

Another question is the nature of the remaining borders which do not correlate with visible changes in cytoarchitecture. Research mainly on nonhuman primates demonstrates that each of the four primary somatosensory areas contains an independent systematic representation of body receptors, corresponding to the well-known somatotopic arrangement: dorsomedial = lower extremity → ventrolateral = oral cavity. The somatotopic maps of areas 3b and 1 are those which are most precise and detailed (Merzenich *et al.*, 1978, 1987; Kaas *et al.*, 1979; Nelson *et al.*, 1980; Sur *et al.*, 1982; Felleman *et al.*, 1983; Cusick *et al.*, 1986). Furthermore, area 3b contains two mosaic-like interdigitated maps, one for slowly adapting and one for rapidly adapting inputs (Sur *et al.*, 1981, 1984). These somatotopic maps of primate S1 have been defined with electrophysiological techniques, i.e., microelectrode recordings. A recent publication showed for the first time in primate S1 that somatotopy is also reflected on a microstructural basis. Brain sections of owl monkey area 3b were cut parallel to the surface and stained for myelin. A mediolateral row of five ovals, separated by myelin-light septa, represented digits and corresponded precisely with cortical sites activated by light touch on individual digits in microelectrode recordings. A more distinct septum separated the hand from the more lateral face representation which could be subdivided into two large myelin-dense ovals that were activated by the upper or lower face in a caudorostral sequence (Jain *et al.*, 1998). The borders within areas 3 and 1 which do not correlate with visible changes in cytoarchitecture may represent cytoarchitectonic equivalents of the fine grained functional organization within areas 3 and 1, i.e., somatotopy and/or cortical representations of different somatosensory receptors. The cytoarchitectonic borders between these entities (note that the study mentioned above used sections stained for myelin) may be so subtle that they can only be resolved with observer-independent techniques. [A technical note: in the sequence of sections from brain 207/84, border 115 in section 3421 most probably corresponds to border 104 in section 3361 and to border 104 in section 3241. A corresponding maximum is missing in section 3301, possibly due to the artifact on the crown of the postcentral gyrus (cf. Fig. 2)].

Interindividual Variability—Implications for Functional Imaging Studies

Two findings of this study are very important for correctly interpreting data from functional imaging studies. First, cytoarchitectonic borders do not match macrostructural landmarks of the postcentral gyrus, i.e., there are no dimples, notches, or grooves which mark borders between cortical areas and which might be visible on high-resolution MR scans. Second, these borders vary considerably in their positions relative to macrostructural landmarks across different brains. Hence, only *genuine* microstructural analysis can define borders between cortical areas.

Therefore, as a next step, these areas will be transformed into the standard anatomical format of the computerized *Human Brain Atlas* (Roland and Zilles, 1994), and corresponding areas from different brains will be superimposed in 3-D space to show the degree of interindividual microstructural variability in a standardized 3-D reference system. On this basis, *genuine* microstructural data can be matched with functional PET or fMRI data (i.e., microstructural-functional correlation on a probabilistic basis).

ACKNOWLEDGMENTS

The authors thank Ms. U. Blohm for excellent technical assistance. Parts of this work were supported by grants from the Deutsche Forschungsgemeinschaft (SFB 194/A6) and the EU BioMed2 and BioTech programs.

REFERENCES

Amunts, K., Schleicher, A., Schormann, T., Bürgel, U., Mohlberg, H., Uylings, H. B. M., and Zilles, K. 1997. The cytoarchitecture of Broca's region and its variability. *NeuroImage* **5:**S353.

Bailey, P., and von Bonin, G. 1951. *The Isocortex of Man*. University of Illinois Press, Urbana, IL.

Braak, H. 1980. *Architectonics of the Human Telencephalic Cortex*. Springer Verlag, Berlin.

Brodmann, K. 1903. Beiträge zur histologischen Lokalisation der Grosshirnrinde. Erste Mitteilung: Die Regio Rolandica. *J. Psychol. Neurol.* **2:**79–107.

Brodmann, K. 1908. Beiträge zur histologischen Lokalisation der Grosshirnrinde. Sechste Mitteilung: Die Cortexgliederung des Menschen. *J. Psychol. Neurol.* **10:**231–246.

Brodmann, K. 1909. *Vergleichende Lokalisationslehre der Grosshirnrinde*. Barth, Leipzig.

Campbell, A. W. 1905. *Histological Studies on the Localization of Cerebral Function*. Cambridge Univ. Press, Cambridge.

Cusick, C. G., Wall, J. T., and Kaas, J. H. 1986. Representations of the face, teeth and oral cavity in areas 3b and 1 of somatosensory cortex in squirrel monkeys. *Brain Res.* **370:**359–364.

Decety, J., Perani, D., Jeannerod, M., Bettinardi, V., Tadary, B., Woods, R., Mazziotta, J. C., and Fazio, F. 1994. Mapping motor representations with positron emission tomography. *Nature* **371:** 600–602.

Duvernoy, H. M., Delon, S., and Vannson, J. L. 1981. Cortical blood vessels of the human brain. *Brain Res. Bull.* **7:**519–579.

Felleman, D. J., Nelson, R. J., Sur, M., and Kaas, J. H. 1983. Representations of the body surface in areas 3b and 1 of postcentral parietal cortex of cebus monkeys. *Brain Res.* **268:**15–26.

Geyer, S., Ledberg, A., Schleicher, A., Kinomura, S., Schormann, T., Bürgel, U., Klingberg, T., Larsson, J., Zilles, K., and Roland, P. E. 1996. Two different areas within the primary motor cortex of man. *Nature* **382:**805–807.

Geyer, S., Ledberg, A., Schormann, T., Zilles, K., and Roland, P. E. 1997. Microstructure and function of the primary somatosensory cortex of man. An integrative study using cytoarchitectonic mapping and PET. *NeuroImage* **5:**S18.

Geyer, S., Zilles, K., Simon, U., Schormann, T., Dabringhaus, A., Schleicher, A., and Roland, P. E. 1995. Architectonic and receptor autoradiographic mapping of the human primary motor cortex. *Hum. Brain Mapp.* **Suppl. 1:**290.

Hallett, M., Fieldman, J., Cohen, L. G., Sadato, N., and Pascual-Leone, A. 1994. Involvement of primary motor cortex in motor imagery and mental practice. *Behav. Brain Sci.* **17:**210.

Iwamura, Y., Iriki, A., and Tanaka, M. 1994. Bilateral hand representation in the postcentral somatosensory cortex. *Nature* **369:** 554–556.

Iwamura, Y., Tanaka, M., and Hikosaka, O. 1980. Overlapping representation of fingers in the somatosensory cortex (area 2) of the conscious monkey. *Brain Res.* **197:**516–520.

Iwamura, Y., Tanaka, M., Sakamoto, M., and Hikosaka, O. 1983a. Converging patterns of finger representation and complex response properties of neurons in area 1 of the first somatosensory cortex of the conscious monkey. *Exp. Brain Res.* **51:**327–337.

Iwamura, Y., Tanaka, M., Sakamoto, M., and Hikosaka, O. 1983b. Functional subdivisions representing different finger regions in area 3 of the first somatosensory cortex of the conscious monkey. *Exp. Brain Res.* **51:**315–326.

Iwamura, Y., Tanaka, M., Sakamoto, M., and Hikosaka, O. 1985. Diversity in receptive field properties of vertical neuronal arrays in the crown of the postcentral gyrus of the conscious monkey. *Exp. Brain Res.* **58:**400–411.

Iwamura, Y., Tanaka, M., Sakamoto, M., and Hikosaka, O. 1993. Rostrocaudal gradients in the neuronal receptive field complexity in the finger region of the alert monkey's postcentral gyrus. *Exp. Brain Res.* **92:**360–368.

Jain, N., Catania, K. C., and Kaas, J. H. 1998. A histologically visible representation of the fingers and palm in primate area 3b and its immutability following long-term deafferentations. *Cereb. Cortex* **8:**227–236.

Kaas, J. H., Nelson, R. J., Sur, M., Lin, C.-S., and Merzenich, M. M. 1979. Multiple representations of the body within the primary somatosensory cortex of primates. *Science* **204:**521–523.

Lashley, K. S., and Clark, G. 1946. The cytoarchitecture of the cerebral cortex of Ateles: A critical examination of architectonic studies. *J. Comp. Neurol.* **85:**223–305.

Leonardo, M., Fieldman, J., Sadato, N., Campbell, G., Ibanez, V., Cohen, L., Deiber, M. P., Jezzard, P., Pons, T., Turner, R., Le Bihan, D., and Hallett, M. 1995. A functional magnetic resonance imaging study of cortical regions associated with motor task execution and motor ideation in humans. *Hum. Brain Map.* **3:**83–92.

Mahalanobis, P. C., Majumda, D. N., and Rao, C. R. 1949. Anthropometric survey of the united provinces: A statistical study. *Sankhya* **9:**89–324.

Merker, B. 1983. Silver staining of cell bodies by means of physical development. *J. Neurosci. Methods* **9:**235–241.

Merzenich, M. M., Kaas, J. H., Sur, M., and Lin, C.-S. 1978. Double representation of the body surface within cytoarchitectonic areas 3b and 1 in "S1" in the owl monkey (*Aotus trivirgatus*). *J. Comp. Neurol.* **181:**41–73.

Merzenich, M. M., Nelson, R. J., Kaas, J. H., Stryker, M. P., Jenkins, W. M., Zook, J. M., Cynader, M. S., and Schoppmann, A. 1987. Variability in hand surface representations in areas 3b and 1 in adult owl and squirrel monkeys. *J. Comp. Neurol.* **258:**281–296.

Morosan, P., Schleicher, A., Schormann, T., and Zilles, K. 1996. Cytoarchitectonic mapping of cortical areas on the first transverse temporal gyrus and intersubject variability. *NeuroImage* **3:**S141.

Mountcastle, V. B. 1997. The columnar organization of the neocortex. *Brain* **120:**701–722.

Nelson, R. J., Sur, M., Felleman, D. J., and Kaas, J. H. 1980. Representations of the body surface in postcentral parietal cortex of *Macaca fascicularis*. *J. Comp. Neurol.* **192:**611–643.

Parsons, L. M., Fox, P. T., Downs, J. H., Glass, T., Hirsch, T. B., Martin, C. C., Jerabek, P. A., and Lancaster, J. L. 1995. Use of implicit motor imagery for visual shape discrimination as revealed by PET. *Nature* **375:**54–58.

Porro, C. A., Francescato, M. P., Cettolo, V., Diamond, M. E., Baraldi, P., Zuiani, C., Bazzocchi, M., and Di Prampero, P. E. 1996. Primary motor and sensory cortex activation during motor performance and motor imagery: A functional magnetic resonance imaging study. *J. Neurosci.* **16:**7688–7698.

Rademacher, J., Caviness, V. S., Steinmetz, H., and Galaburda, A. M. 1993. Topographical variation of the human primary cortices: Implications for neuroimaging, brain mapping, and neurobiology. *Cereb. Cortex* **3:**313–329.

Rademacher, J., Werner, C., Morosan, P., Schleicher, A., Zilles, K., and Steinmetz, H. 1996. Localization and variability of cytoarchitectonic areas in the human superior temporal cortex. *NeuroImage* **3:**S456.

Rajkowska, G., and Goldman-Rakic, P. S. 1995. Cytoarchitectonic definition of prefrontal areas in the normal human cortex. II. Variability in locations of areas 9 and 46 and relationship to the Talairach coordinate system. *Cereb. Cortex* **5:**323–337.

Rao, S. M., Binder, J. R., Bandettini, P. A., Hammeke, T. A., Yetkin, F. Z., Jesmanowicz, A., Lisk, L. M., Morris, G. L., Mueller, W. M., Estkowski, L. D., Wong, E. C., Haughton, V. M., and Hyde, J. S.

1993. Functional magnetic resonance imaging of complex human movements. *Neurology* **43:**2311–2318.

Roland, P. E., Geyer, S., Amunts, K., Schormann, T., Schleicher, A., Malikovic, A., and Zilles, K. 1997. Cytoarchitectural maps of the human brain in standard anatomical space. *Hum. Brain Map.* **5:**222–227.

Roland, P. E., Larsen, B., Lassen, N. A., and Skinhoj, E. 1980. Supplementary motor area and other cortical areas in organization of voluntary movements in man. *J. Neurophysiol.* **43:**118–136.

Roland, P. E., and Zilles, K. 1994. Brain atlases—A new research tool. *Trends Neurosci.* **17:**458–467.

Roland, P. E., and Zilles, K. 1996. Functions and structures of the motor cortices in humans. *Curr. Opin. Neurobiol.* **6:**773–781.

Roth, M., Decety, J., Raybaudi, M., Massarelli, R., Delon-Martin, C., Segebarth, C., Morand, S., Gemignani, A., Décorps, M., and Jeannerod, M. 1996. Possible involvement of primary motor cortex in mentally simulated movement: A functional magnetic resonance imaging study. *Neuroreport* **7:**1280–1284.

Sabbah, P., Simond, G., Levrier, O., Habib, M., Trabaud, V., Murayama, N., Mazoyer, B. M., Briant, J. F., Raybaud, C., and Salamon, G. 1995. Functional magnetic resonance imaging at 1.5 T during sensorimotor and cognitive task. *Eur. Neurol.* **35:**131–136.

Sanes, J. N. 1994. Neurophysiology of preparation, movement and imagery. *Behav. Brain Sci.* **17:**221–223.

Sarkissov, S. A., Filimonoff, I. N., Kononowa, E. P., Preobraschenskaja, I. S., and Kukuew, L. A. 1955. *Atlas of the Cytoarchitectonics of the Human Cerebral Cortex.* Medgiz, Moscow.

Schleicher, A., Amunts, K., Geyer, S., Morosan, P., and Zilles, K. 1999. Observer-independent method for microstructural parcellation of cerebral cortex: A quantitative approach to cytoarchitectonics. *NeuroImage*, **9:**165–177.

Schleicher, A., Amunts, K., Geyer, S., Simon, U., Zilles, K., and Roland, P. E. 1995. A method of observer-independent cytoarchitectonic mapping of the human cortex. *Hum. Brain Map.* **Suppl. 1:**77.

Schleicher, A., and Zilles, K. 1990. A quantitative approach to cytoarchitectonics: Analysis of structural inhomogeneities in nervous tissue using an image analyser. *J. Microsc.* **157:**367–381.

Simon, U., Geyer, S., Zilles, K., Schormann, T., Dabringhaus, A., Schleicher, A., and Roland, P. E. 1995. Architectonic and receptor autoradiographic mapping of the human primary somatosensory cortex. *Hum. Brain Map.* **Suppl. 1:**259.

Stephan, K. M., Fink, G. R., Passingham, R. E., Silbersweig, D., Ceballos-Baumann, A. O., Frith, C. D., and Frackowiak, R. S. J. 1995. Functional anatomy of the mental representation of upper extremity movements in healthy subjects. *J. Neurophysiol.* **73:**373–386.

Sur, M., Nelson, R. J., and Kaas, J. H. 1982. Representations of the body surface in cortical areas 3b and 1 of squirrel monkeys: Comparisons with other primates. *J. Comp. Neurol.* **211:**177–192.

Sur, M., Wall, J. T., and Kaas, J. H. 1981. Modular segregation of functional cell classes within the postcentral somatosensory cortex of monkeys. *Science* **212:**1059–1061.

Sur, M., Wall, J. T., and Kaas, J. H. 1984. Modular distribution of neurons with slowly adapting and rapidly adapting responses in area 3b of somatosensory cortex in monkeys. *J. Neurophysiol.* **51:**724–744.

Van Essen, D. C. 1997. A tension-based theory of morphogenesis and compact wiring in the central nervous system. *Nature* **385:**313–318.

Vogt, C., and Vogt, O. 1919. Allgemeinere Ergebnisse unserer Hirnforschung. *J. Psychol. Neurol.* **25:**279–461.

von Economo, K., and Koskinas, G. 1925. *Die Cytoarchitektonik der Hirnrinde des erwachsenen Menschen.* Springer Verlag, Wien.

White, L. E., Andrews, T. J., Hulette, C., Richards, A., Groelle, M., Paydarfar, J., and Purves, D. 1997. Structure of the human sensorimotor system. I. Morphology and cytoarchitecture of the central sulcus. *Cereb. Cortex* **7:**18–30.

Wree, A., Schleicher, A., and Zilles, K. 1982. Estimation of volume fractions in nervous tissue with an image analyzer. *J. Neurosci. Methods* **6:**29–43.

Zilles, K., Schleicher, A., Langemann, C., Amunts, K., Morosan, P., Palomero-Gallagher, N., Schormann, T., Mohlberg, H., Bürgel, U., Steinmetz, H., Schlaug, G., and Roland, P. E. 1997. Quantitative analysis of sulci in the human cerebral cortex: Development, regional heterogeneity, gender difference, asymmetry, intersubject variability and cortical architecture. *Hum. Brain Map.* **5:**218–221.